BIOCHEMISTRY

Mechanism of actin N-terminal acetylation

Grzegorz Rebowski[1]*, Malgorzata Boczkowska[1]*, Adrian Drazic[2], Rasmus Ree[2], Marianne Goris[3], Thomas Arnesen[2,3,4], Roberto Dominguez[1]†

About 80% of human proteins are amino-terminally acetylated (Nt-acetylated) by one of seven Nt-acetyltransferases (NATs). Actin, the most abundant protein in the cytoplasm, has its own dedicated NAT, NAA80, which acts post-translationally and affects cytoskeleton assembly and cell motility. Here, we show that NAA80 does not associate with filamentous actin in cells, and its natural substrate is the monomeric actin-profilin complex, consistent with Nt-acetylation preceding polymerization. NAA80 Nt-acetylates actin-profilin much more efficiently than actin alone, suggesting that profilin acts as a chaperone for actin Nt-acetylation. We determined crystal structures of the NAA80-actin-profilin ternary complex, representing different actin isoforms and different states of the catalytic reaction and revealing the first structure of NAT-substrate complex at atomic resolution. The structural, biochemical, and cellular analysis of mutants shows how NAA80 has evolved to specifically recognize actin among all cellular proteins while targeting all six actin isoforms, which differ the most at the amino terminus.

INTRODUCTION

N-terminal acetylation (Nt-acetylation) is a prevalent modification that affects ~80% of human proteins and can have a major impact on human health and disease (*1*–*4*). The reaction is catalyzed by one of seven Nt-acetyltransferases (NATs) (NatA to NatF and NatH), whose catalytic subunits (NAA10 to NAA60 and NAA80) display a common fold but low sequence identity. The NATs transfer the acetyl group ($COCH_3$) from acetyl coenzyme A (AcCoA) onto the free N-terminal α-amino group of their protein substrates. Five of the NATs (NatA to NatE) associate with the ribosome and act cotranslationally, whereas NatF binds to the Golgi membrane and Nt-acetylates transmembrane proteins (*5*). Most NATs are rather promiscuous, acting on large subsets of proteins. One exception is NatD, which Nt-acetylates only two substrates, histones H2A and H4 (*6*). In addition, we recently found that actin, the most abundant protein in the cytoplasm of eukaryotic cells, has its own dedicated NAT, NAA80 (*7*). Actin Nt-acetylation is also unique in that it proceeds through a multistep mechanism that involves both co- and posttranslational modification (*8*, *9*). During translation, the initiator methionine (iMet) of the two cytoplasmic actin isoforms is Nt-acetylated, whereas the iMet of the four-muscle actin isoforms is removed and the exposed cysteine is Nt-acetylated by one of the ribosome-associated NATs. This is followed by the removal of the N-terminal Ac-Met (or Ac-Cys) by a still unidentified acetylaminopeptidase. Then, all six actin isoforms, which at this point carry either three (cytoplasmic β/γ-actin and smooth muscle γ-actin) or four (muscle α-actin isoforms) negatively charged amino acids at the N terminus, are posttranslationally Nt-acetylated by NAA80 (*7*, *10*). NAA80 is highly specific, targeting only actin among all the proteins in the cell, whereas its knockout (KO) completely abolishes actin Nt-acetylation, showing that no other NAT can substitute for NAA80. Actin's acetylated N terminus is prominently exposed in the actin filament where it can interact with many filamentous actin-binding proteins (ABPs) (*9*), and consistently, actin Nt-acetylation critically affects filament assembly in vitro and in cells. In vitro, the absence of Nt-acetylation leads to a decrease in the rates of filament depolymerization and elongation, including formin-induced elongation, whereas *NAA80* KO cells display increased filopodia and lamellipodia formation and accelerated cell motility (*7*, *9*). Here, we describe the mechanism of actin Nt-acetylation by NAA80. Biochemical, structural, and cellular data show how NAA80 has evolved to specifically recognize the complex of actin-profilin while being able to Nt-acetylate all six actin isoforms, which diverge the most at the N terminus.

RESULTS

NAA80 targets monomeric actin in vitro and in cells

The seven human NATs have a common catalytic core, but they share low sequence conservation, with NAA80 being the most divergent of them all (fig. S1). NAA80 shares only 16.9% sequence identity with its closest relative, NAA20, and contains a divergent 77–amino acid N-terminal extension and a unique 70–amino acid Pro-rich loop inserted before the last β-strand of the catalytic domain (Fig. 1A). N- and C-terminal extensions are common among the NATs and are typically implicated in the recruitment of auxiliary subunits that regulate the catalytic activity and subcellular localization (*2*). We asked whether NAA80's N-terminal extension plays a role in its activity and/or localization and whether NAA80 targets monomeric (G-actin) or filamentous (F-actin) actin in cells.

In vitro, we found that full-length NAA80 ($NAA80_{FL}$) and a construct lacking the N-terminal extension, residues 78 to 308 ($NAA80_{\Delta N}$), can both Nt-acetylate β/γ-actin purified from *NAA80* KO HAP1 cells, as confirmed by Western blot analysis with isoform- and Nt-acetylation–specific anti–Ac-β-actin antibodies (Fig. 1B). In cells, the expression of green fluorescent protein (GFP)–$NAA80_{\Delta N}$, but not GFP alone, rescued β/γ-actin acetylation in *NAA80* KO cells (Fig. 1C). Thus, while the N-terminal extension may play a role in localization and/or modulation of the catalytic activity, it appears to be dispensable for Nt-acetylation in vitro and in cells.

We then performed cell fractionation assays to assess whether NAA80 associates with the soluble, G-actin–containing, or the pellet, F-actin–containing, fraction in cells. Endogenous NAA80 was found predominantly in the soluble fraction, analogous to profilin,

[1]Department of Physiology, Perelman School of Medicine, University of Pennsylvania, Philadelphia, PA, USA. [2]Department of Biomedicine, University of Bergen, Bergen, Norway. [3]Department of Biological Sciences, University of Bergen, Bergen, Norway. [4]Department of Surgery, Haukeland University Hospital, Bergen, Norway.
*These authors contributed equally to this work.
†Corresponding author. Email: droberto@pennmedicine.upenn.edu

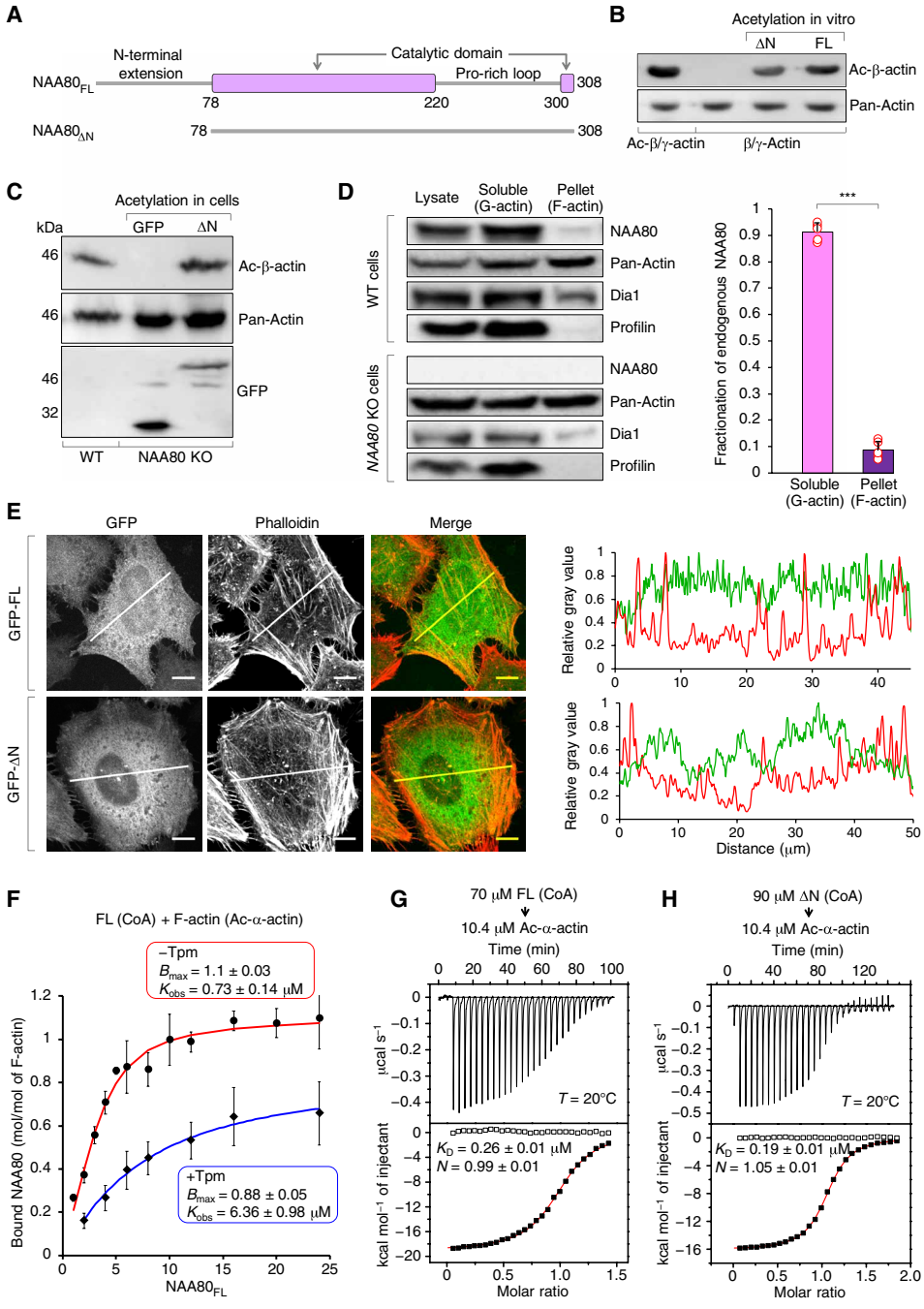

Fig. 1. NAA80 preferentially binds monomeric actin in vitro and in cells. (**A**) Domain diagram of NAA80, showing the two major constructs used in this study. (**B**) In vitro acetylation by $NAA80_{\Delta N}$ (lacking the 77–amino acid N-terminal extension, or ΔN) of nonacetylated β/γ-actin analyzed by Western blotting, using acetylation- and isoform-specific anti–Ac-β-actin antibody. Ac-β/γ-actin purified from WT cells and actin acetylated by full-length NAA80 ($NAA80_{FL}$ or FL) were used as controls. Loading was controlled by anti–pan-actin staining. (**C**) Rescue of acetylation in *NAA80* KO cells by $NAA80_{\Delta N}$ analyzed as in (B). Lysate from WT cells was used as a control. Anti–green fluorescent protein (GFP) staining confirmed $NAA80_{\Delta N}$ expression in cells. (**D**) Western blot analysis of the presence of endogenous NAA80 in the soluble (G-actin) and pellet (F-actin) fractions of HAP1 WT cells using custom anti-NAA80 antibody (1:200). Controls are profilin, which binds only G-actin, and Dia1, which binds both G- and F-actin. *NAA80* KO cells are shown as a control for custom antibody specificity. Left: Representative Western blots (fig. S8). Right: Quantifications, showing data points (red circles) and means ± SD ($n = 5$). The statistical significance of the data was determined using an unpaired two-sided Student's t test (***$P < 0.001$). (**E**) Representative HeLa cells expressing GFP-$NAA80_{FL}$ (GFP-FL) or GFP-$NAA80_{\Delta N}$ (GFP-ΔN) and stained with Alexa Fluor 546 phalloidin to visualize F-actin. Scale bar, 10 μm. Line scans illustrate the lack of NAA80 colocalization with F-actin, as also confirmed by whole-cell correlation coefficient analysis on $n = 15$ cells (fig. S2, D and E). (**F**) Cosedimentation of $NAA80_{FL}$ with F-actin (Ac-α-actin) ± tropomyosin (Tpm). Data points correspond to the mean from three independent experiments ± SEM (fig. S7A). The maximum molar binding ratio (B_{max}) and observed dissociation constant (K_{obs}) were calculated using a nonlinear least square fit (see Materials and Methods). (**G** and **H**) Isothermal titration calorimetry (ITC) titrations of $NAA80_{FL}$ and $NAA80_{\Delta N}$ (CoA) into Ac-α-actin (latrunculin B, or LatB), using the indicated experimental conditions. The dissociation constant (K_D) and binding stoichiometry (N) were derived from fitting to a one-site binding isotherm (red line). Errors correspond to the SD of the fits. Open symbols correspond to control titrations into buffer.

a prototypical G-actin–binding protein (Fig. 1D). In contrast, the formin Dia1, which can bind both G- and F-actin, appeared in the soluble and pellet fractions. We also analyzed three V5-tagged constructs ($NAA80_{FL}$, $NAA80_{\Delta N}$, and the catalytically inactive mutant $NAA80_{CM}$) expressed in wild-type (WT) and *NAA80* KO cells. Analogous to endogenous NAA80, all three constructs were predominantly associated with the soluble fraction (fig. S2A). We note, however, that $NAA80_{\Delta N}$ was slightly more likely to be found in the pellet fraction, suggesting that the N-terminal tail of NAA80 interferes somewhat with binding to F-actin in cells. The relative amount of endogenous and exogenously expressed $NAA80_{FL}$ in the pellet fraction was always less than 10%, even when their relative abundance was approximately 1:1200 (fig. S2B). It thus appears that NAA80 does not associate with the F-actin–containing fraction even when present at high levels.

Consistent with these results, constructs GFP-$NAA80_{FL}$ and GFP-$NAA80_{\Delta N}$ expressed in HeLa cells did not colocalize with Alexa Fluor 546 phalloidin–stained F-actin fibers and displayed a cytosolic localization similar to that of the mCherry control (Fig. 1E and fig. S2D). This result was corroborated through whole-cell quantification of the amount of overlap between the fluorescent intensities of GFP and Alexa Fluor 546 (or mCherry) (fig. S2E). GFP-$NAA80_{FL}$ also did not colocalize with mitochondria (DsRed-Mito) and endoplasmic reticulum (mCherry-Sec61B and mCherry-calnexin) markers and appeared to be excluded from these organelles (fig. S2F).

Combined, these observations suggest that NAA80 associates with the G-actin and not the F-actin pool in cells. Moreover, this localization is mostly independent of the presence/absence of the N-terminal extension of NAA80 or whether actin is Nt-acetylated. Construct $NAA80_{CM}$ that fails to rescue actin Nt-acetylation in *NAA80* KO cells (*7*) was also found in the G-actin fraction (fig. S2A).

Next, we tested binding of NAA80 to G- and F-actin in vitro. In these experiments, we first used α-skeletal actin, which is N-terminally acetylated (Ac-α-actin), and NAA80 with CoA bound. In cosedimentation assays, NAA80 bound F-actin with an observed dissociation constant (K_{obs}) of 0.73 μM (Fig. 1F), which contrasted with the apparent lack of binding in cells. A recent study, however, suggests that most actin filaments in cells are associated with tropomyosin (Tpm) (*11*), which acts as the gatekeeper of the actin filament (*12*). To test whether Tpm competes with NAA80 for binding to F-actin, we performed cosedimentation assays with Tpm-decorated filaments. Tpm reduced the affinity of NAA80 for F-actin approximately ninefold (K_{obs} of 6.4 μM), suggesting at least partial competition (Fig. 1F and see Discussion).

Binding to G-actin was quantitatively assessed using isothermal titration calorimetry (ITC). In these experiments (Fig. 1, G and H), latrunculin B (LatB) was used to prevent actin polymerization. Both, $NAA80_{FL}$ and $NAA80_{\Delta N}$ bound Ac-α-actin with similarly high affinities (dissociation constant, K_D of 0.26 and 0.19 μM, respectively) and ~1:1 stoichiometry, suggesting that the N-terminal extension does not participate in actin binding. Therefore, NAA80 has substantially higher affinity for G- than F-actin, particularly considering that in cells, competition with Tpm is likely, which might explain the lack of colocalization with F-actin.

Profilin acts as a chaperone for actin Nt-acetylation by NAA80

In cells, the G-actin pool exists mostly in the form of complexes with ABPs (*13*, *14*). Therefore, we tested the ability of NAA80 to bind to some of the most common actin-ABP complexes. By ITC, $NAA80_{\Delta N}$ (CoA) failed to bind the complexes of Ac-α-actin with gelsolin segment 1 (GS1) and thymosin β4, suggesting direct competition with these two proteins (fig. S3, A, B, and D). In contrast, $NAA80_{\Delta N}$ (CoA) bound with high-affinity the complex of Ac-α-actin with deoxyribonuclease I (DNase I) (fig. S3C).

Profilin is the most abundant ABP in cells (*13*). With a cellular concentration of 50 to 100 μM, a high affinity for adenosine triphosphate (ATP)–G-actin (K_D of 0.1 μM) (*15*), as well as the ability to compete with Tβ4 for binding to actin monomers (*16*), profilin-actin accounts for the largest fraction of monomeric actin in cells (*13*). Both $NAA80_{FL}$ and $NAA80_{\Delta N}$ bound the complex of Ac-α-actin–profilin with similarly high affinities (K_D of 0.23 and 0.15 μM, respectively) (Fig. 2, A and B). This result also suggests that the N-terminal extension of NAA80 is not necessary for binding to actin-profilin.

Since NAA80 targets the N terminus of actin, which varies among isoforms, we asked whether its preference for the monomer was also observed with β/γ-actin. In cosedimentation assays, $NAA80_{FL}$ bound the Ac-β/γ-actin filament with a K_{obs} of 5.2 μM (Fig. 2C), whereas by ITC, $NAA80_{\Delta N}$ bound both Ac-β/γ-actin–profilin and nonacetylated β/γ-actin–profilin with ~2.5-fold higher affinity (K_D of 2.4 and 1.8 μM, respectively) (Fig. 2, D and E). While these measurements confirm NAA80's preference for the monomer, independent of actin isoform, it is interesting that NAA80 binds α-actin (both monomer and filament) with ~16-fold higher affinity than β/γ-actin (Fig. 2, B and D), showing the importance of actin's variable N terminus for recognition by NAA80.

Pro-rich sequences are abundant among cytoskeletal proteins and are typically implicated in the binding of profilin or SH3-containing proteins (*17*). The Pro-rich loop of NAA80 contains a canonical profilin-binding site (^{261}PPLPPPPPLP^{270}) (*18*, *19*), suggesting that NAA80 may interact directly with profilin. Consistent with this idea, $NAA80_{\Delta N}$ bound profilin with ~1:1 stoichiometry (Fig. 2F), albeit with relatively low affinity (K_D of 30 μM), which is similar to other profilin interactions with Pro-rich sequences (*18*, *19*).

Together, these results suggest that actin-profilin, not just actin, is the preferred NAA80 substrate. To further test this idea, we asked whether profilin modulates the catalytic activity of NAA80 toward actin. We compared the extent of Nt-acetylation of β/γ-actin purified from *NAA80* KO cells alone and in complex with profilin using isoform- and acetylation-specific anti–β-actin antibodies. The presence of profilin significantly enhanced the Nt-acetylation efficiency of NAA80 as a function of reaction time and enzyme:substrate ratio (Fig. 2G). Together, the results presented here suggest that profilin acts as a chaperone for actin Nt-acetylation. Moreover, Nt-acetylation is likely to occur before polymerization since profilin acts as the main carrier of actin monomers into filaments due to its ability to bind Pro-rich sequences in actin assembly factors such as formins and vasodilator-stimulated phosphoprotein (VASP) (*13*, *14*).

The NAA80 structure is specifically adapted to recognize the actin-profilin complex

So far, a structure of a NAT bound to its entire substrate had not been determined, possibly because the NATs are rather promiscuous and bind their substrates transiently during translation (*2*). The specificity and relatively high affinity of NAA80 for its substrate allowed us to obtain three structures of the ternary complex of

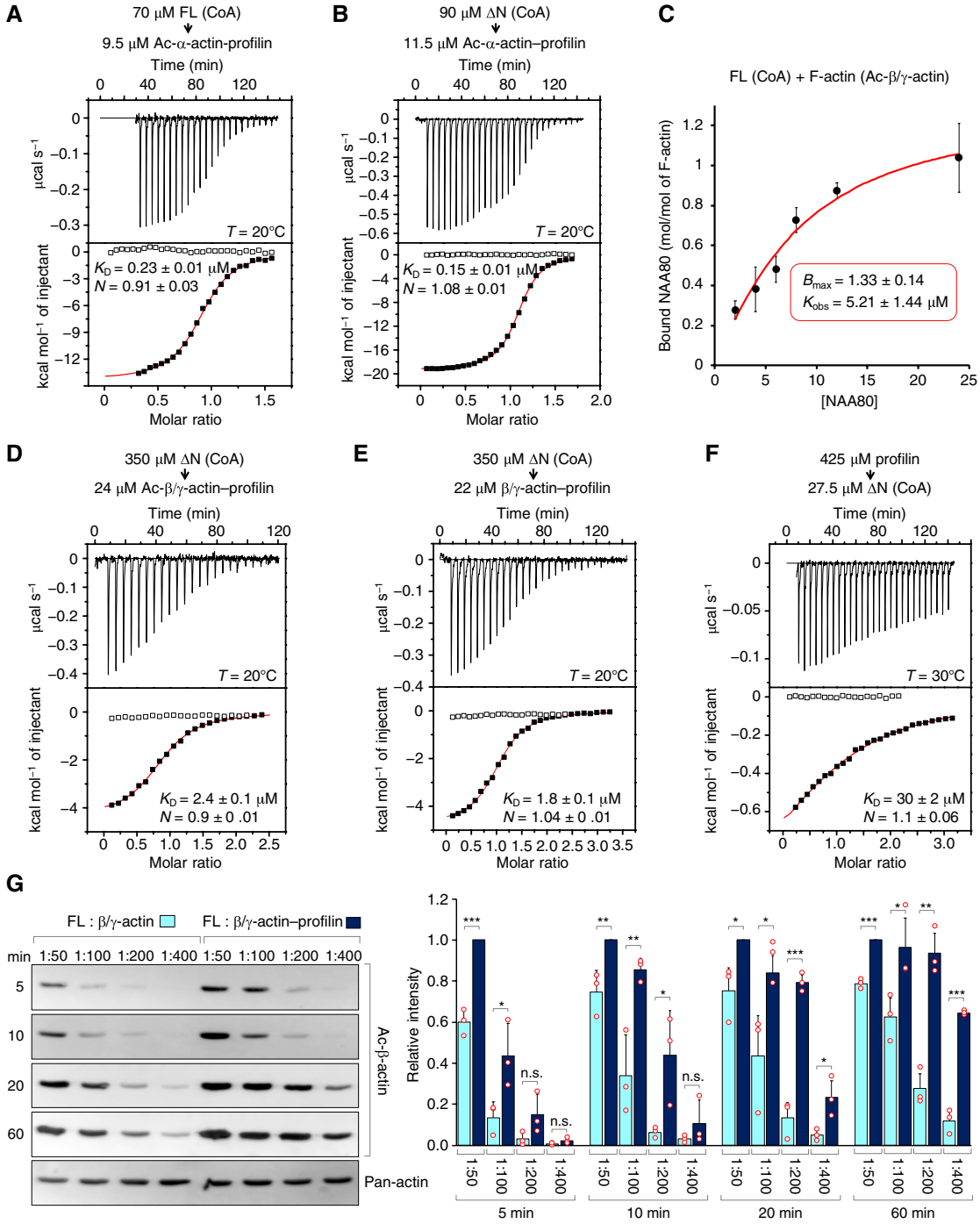

Fig. 2. Complex of actin-profilin is a preferred substrate of NAA80. (**A** and **B**) ITC titrations of $NAA80_{FL}$ (FL) and $NAA80_{\Delta N}$ (ΔN) with bound CoA into Ac-α-actin–profilin (LatB) using the indicated experimental conditions. The K_D and binding stoichiometry (*N*) were derived from fitting to a one-site binding isotherm (red line). Errors correspond to the SD of the fits. Open symbols correspond to control titrations into buffer. (**C**) Cosedimentation of $NAA80_{FL}$ with F-actin (Ac-β/γ-actin). Data points correspond to the mean from three independent experiments ± SEM (fig. S7B). The maximum molar binding ratio (B_{max}) and K_{obs} were calculated using a nonlinear least square fit. (**D** and **E**) ITC titrations of $NAA80_{\Delta N}$ (CoA) into acetylated and nonacetylated β/γ-actin-profilin (LatB), using the indicated experimental conditions. The K_D and binding stoichiometry (*N*) were derived from fitting to a one-site binding isotherm (red line). Errors correspond to the SD of the fits. Open symbols correspond to control titrations into buffer. (**F**) ITC titrations of profilin into $NAA80_{\Delta N}$ (CoA), using the indicated experimental conditions and analyzed as above. (**G**) In vitro acetylation of 10 μM nonacetylated β/γ-actin alone or in complex with profilin by $NAA80_{FL}$, analyzed by Western blotting using acetylation- and isoform-specific anti–Ac-β-actin antibody. The conditions of the acetylation reaction ($NAA80_{FL}$:actin or $NAA80_{FL}$:actin-profilin ratio and time) are indicated in the figure. Loading was controlled by anti–pan-actin staining. Left: Representative Western blot. Right: Quantification from three independent experiments. For each blot, the band intensities were normalized to the 1:50 $NAA80_{FL}$:actin-profilin band. Shown are mean relative intensities ± SD ($n = 3$) and individual data points (red open circles). The statistical significance was determined using an unpaired two-sided Student's *t* test [not significant (n.s.), $P \geq 0.05$, $^*P < 0.05$, $^{**}P < 0.01$, $^{***}P < 0.001$].

$NAA80_{\Delta N}$ with actin-profilin, corresponding to different steps along the catalytic pathway and different actin isoforms (Fig. 3, Table 1, fig. S4, and movie S1). One structure represents the first step in the catalytic reaction, i.e., before the acetyl group is transferred onto the protein substrate. This structure contains nonacetylated β/γ-actin (i.e., a mixture of the two cytoplasmic isoforms purified from *NAA80* KO cells) in complex with profilin and $NAA80_{\Delta N}$ with bound acetonyl-CoA (AnCoA), a nonhydrolyzable AcCoA analog. The second structure is that of Ac-α-actin–profilin in complex with $NAA80_{\Delta N}$ (CoA), corresponding to a state in which the acetyl group has already been transferred onto the actin substrate. This structure has the highest resolution (2.0 Å) among the three described here (Table 1) and is thus used in most illustrations. The third structure is that of Ac-α-actin–profilin in complex with $NAA80_{\Delta N}$ (AcCoA), representing the last step in the catalytic reaction, i.e., the release of the protein substrate prompted by NAA80 reloading with AcCoA. In this structure, the acetyl groups on AcCoA and actin sterically hinder one another, and, consequently, the affinity of NAA80 for Ac-α-actin–profilin is ~8.5-fold lower (K_D of 1.7 μM) with AcCoA than with CoA (compare Fig. 2A and fig. S4D).

The three structures are very similar, with the most important differences centered around the variable N termini of actin (fig. S4, A to C). NAA80 buries a large surface of 4160 $Å^2$ on actin-profilin (3199 $Å^2$ on actin and 961 $Å^2$ on profilin). For comparison, profilin buries a surface of 2630 $Å^2$ on actin. The NAA80-binding surface can be conceptually divided into three areas: the profilin-binding site, the actin-binding surface, and the actin N-terminus–binding site (Fig. 3 and movie S1). The profilin-binding site appears to be mostly conserved between the two major profilin isoforms (1 and 2), although it contributes modestly to the overall binding affinity of NAA80 to actin-profilin (Fig. 2F).

NAA80 interacts almost exclusively with actin subdomain 1, contacting a surface that is both conserved among actin isoforms and highly specific for NAA80. Actin is highly conserved from yeast to humans, and sequence identity among the six human isoforms ranges from 93.3 to 98.9% (*9*). In contrast, sequence identity among the seven human NATs is low, ranging from 7.9 to 29.9% (fig. S1). As a result, the surface that actin presents to NAA80 is strictly conserved (Fig. 3B), whereas the counterpart surface on NAA80 is highly variable among the NATs (Fig. 3C) but tailored specifically for actin binding through adaptations of the sequence and structure, including repositioning of the loop-helix T105-Q118, the absence of β-strand 6, a unique loop Q294-P300, and charge complementarity with actin (fig. S5, A and B).

The N terminus is the most variable region among actin isoforms, and it is one amino acid shorter in cytoplasmic β/γ-actin than in skeletal α-actin (Figs. 3B and 4A). In most actin structures, the N terminus is disordered, whereas in the structures described here, it adopts an extended conformation along one-half of the catalytic cleft of NAA80, with the other half being occupied by the AcCoA derivative (Fig. 3A and fig. S4, A to C). Among the NATs, the region of the cleft that binds the substrate N terminus is variable, whereas the AcCoA-binding site is conserved (Fig. 3C). The actin N terminus is well defined in the electron density maps of the two structures containing Ac-α-actin, whereas the nonacetylated N terminus of β/γ-actin is less well resolved, which is probably due to the presence of a mixture of isoforms in this structure (fig. S4A). In nonmuscle cells, cytoplasmic β- and γ-actin are typically found at a ratio of 2:1 (*20*), and thus, we modeled the N terminus of the nonacetylated structure using the more abundant β-actin sequence. Despite these ambiguities, the N termini of β/γ-actin seem to bind NAA80 in a similar manner to that of Ac-α-actin (fig. S4). In support of this conclusion, CoA and the first three amino acids of Ac-α-actin superimpose well with a bisubstrate analog consisting of AcCoA covalently attached to the first four amino acids of β-actin, as observed in a recent structure of *Drosophila* NAA80 (fig. S5, C and D) (*21*). Only the fourth amino acid of the bisubstrate analog displays a different orientation than that of the natural actin substrate. More generally, the catalytic core of *Drosophila* NAA80 superimposes well with that of human NAA80 (a root mean square deviation of 0.82 Å for 119 equivalent Cα atoms) despite the absence of a bound substrate in the *Drosophila* structure and considering that the two proteins share only 30% sequence identity. *Drosophila* NAA80 also lacks the N-terminal extension and the Pro-rich loop (fig. S5C), suggesting that in *Drosophila*, profilin is unlikely to play a role in actin Nt-acetylation.

NAA80 is specifically adapted to recognize all six actin isoforms

In NAA80, the region of the catalytic site that binds the actin N terminus is shaped in the form of an open cleft, as opposed to a narrow tunnel in other NATs (*21*), and it is also positively charged, which counters actin's negatively charged N terminus (Fig. 3, B and C, and fig. S5B). The charge complementarity between actin and NAA80 extends beyond the N terminus–binding site, with the entire contact surface being predominantly negatively charged in actin and positively charged in NAA80 (Fig. 3, B and C). In this way, NAA80 appears to have evolved a catalytic cleft adapted to recognize the variable but negatively charged N termini of the actin isoforms, whereas other contacts appear to specifically adapt this enzyme for recognition of a single substrate in the cell, actin-profilin.

To further test this idea, we asked whether NAA80 could acetylate N-terminal peptides from other actin isoforms. We found that NAA80 expressed in either mammalian cells or *Escherichia coli* was able to effectively acetylate N-terminal peptides from the six actin isoforms expressed in humans but not a prototypical NatA/NAA10-substrate peptide (Fig. 4B). This result confirms the specificity of NAA80 for actin N-terminal peptides independent of isoform and expands upon previous studies that showed NAA80's ability to Nt-acetylate cytoplasmic β- and γ-actin and skeletal α-actin (*7*, *22*). These data also suggest that NAA80 has lower catalytic efficiency toward the skeletal α-actin peptide. We cannot be sure that the differences in NAA80's catalytic efficiency toward N-terminal peptides hold true for the full-length substrates. Yet, we have shown here that $NAA80_{\Delta N}$ (CoA) interacts ~16-fold more tightly with skeletal Ac-α-actin–profilin than cytoplasmic Ac-β/γ-actin–profilin (Fig. 2, B and D), suggesting that substrate release after Nt-acetylation may be slower for Ac-α-actin–profilin, thus resulting in reduced Nt-acetylation efficiency toward this isoform. In muscle sarcomeres, α-actin has a particularly long half-life of ~20 days (*23*), such that a somewhat reduced efficiency of NAA80 toward this isoform is unlikely to become a limiting factor in vivo.

Next, we tested the in vitro and cellular activity of four NAA80 mutants (M1 to M4) targeting groups of amino acids on the actin-profilin–binding surface (Fig. 4C). As expected, these mutants, which leave the catalytic cleft intact, had approximately the same in vitro activity as WT NAA80 toward N-terminal peptides corresponding to the three actin isoforms present in the structures (Fig. 4D).

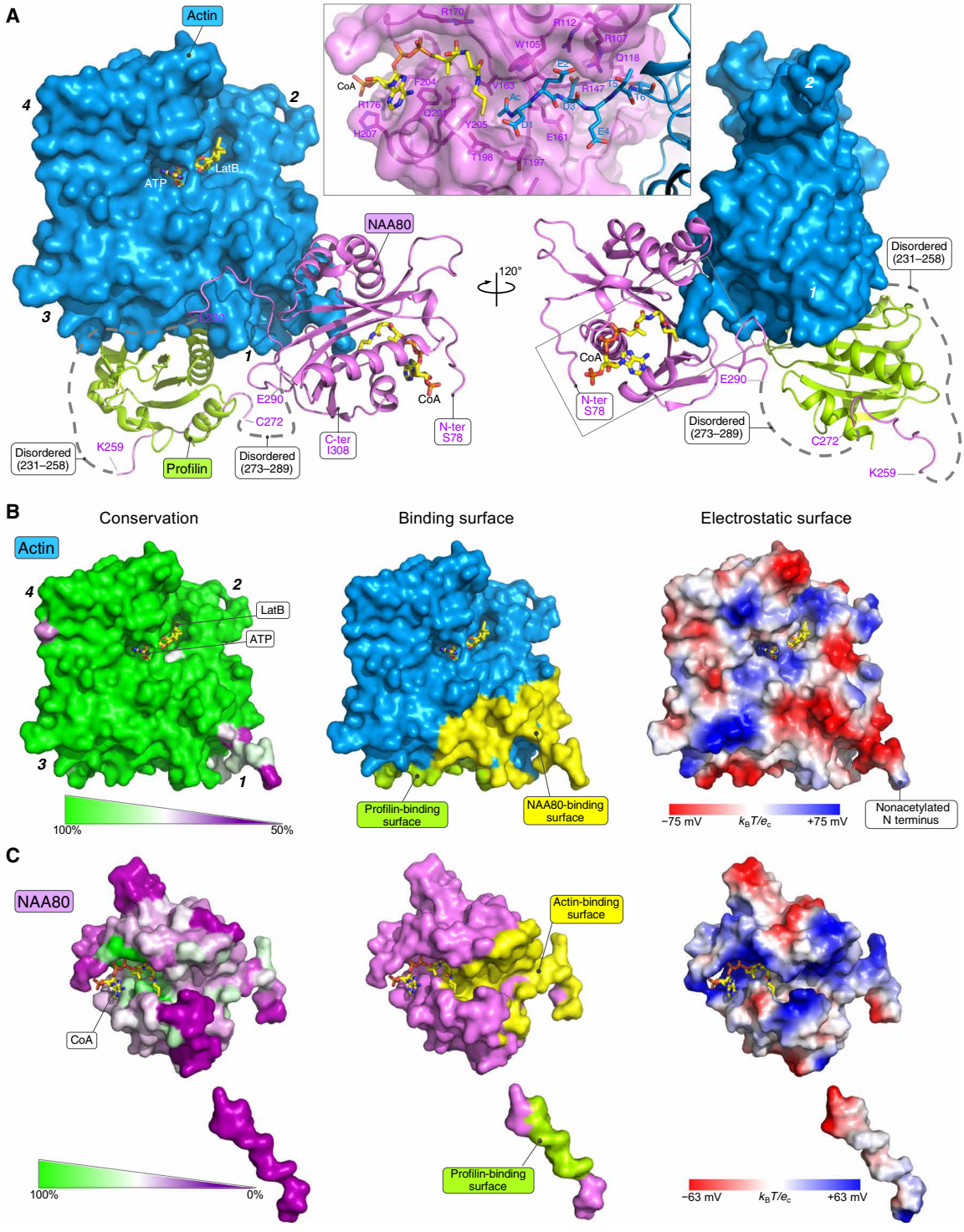

Fig. 3. Structural basis of NAA80 binding to actin-profilin. (**A**) Structure of the ternary complex of $NAA80_{\Delta N}$ (ΔN) with CoA bound (magenta), Ac-α-actin (LatB; blue), and profilin (green). Gray broken lines illustrate two flexible regions of NAA80 that were not visualized in the electron density map. A zoom in the middle highlights the catalytic cleft of NAA80 (indicated by a rectangle), showing CoA and the acetylated N terminus of α-actin. Key amino acids are numbered. (**B** and **C**) Analysis of actin-NAA80 contact interface according to sequence conservation and charge complementarity. Conservation scores (fig. S1) were plotted onto the surfaces of Ac-α-actin and NAA80 derived from the structure of their complex. Amino acid conservation decreases from green to magenta (as indicated), using a conservation range of 100 to 50% for actins (which are highly conserved) and 100 to 0% for the NATs (which are poorly conserved). The contact surfaces on actin (blue) and NAA80 (magenta) are highlighted yellow, and the profilin contact surface is highlighted green. Actin subdomains are numbered 1 to 4 (bold, italic characters). NAA80 interacts almost exclusively with actin subdomain 1, whose surface is predominantly negatively charged, whereas the counterpart contact surface on NAA80 is mostly positively charged, as revealed by their respective electrostatic-surface representations. See also movie S1.

Table 1. Crystallographic data and refinement statistics.

Structure	Ac-α-actin–profilin–NAA80$_{\Delta N}$ (CoA)	Ac-α-actin–profilin–NAA80$_{\Delta N}$ (AcCoA)	β/γ-actin–profilin–NAA80$_{\Delta N}$ (AnCoA)
Data collection			
Beamline	MacCHESS F1	MacCHESS F1	MacCHESS F1
Date data collection	11/27/2017	11/27/2017	11/27/2017
Wavelength (Å)	0.977	0.977	0.977
Space group	$C222_1$	$C222_1$	$C222_1$
Cell *a*, *b*, *c* (Å)	104.5, 115.9, 132.5	103.8, 114.9, 132.3	104.4, 115.6, 132.2
Cell α, β, γ (°)	90, 90, 90	90, 90, 90	90, 90, 90
Resolution (Å)	50.0–2.0 (2.07–2.0)	50.0–2.9 (3.0–2.9)	50.0–2.5 (2.59–2.5)[a]
R_{merge} (%)	9.3 (57.6)	17.3 (55.8)	11.6 (56.3)
$I/\sigma I$	30.2 (4.5)	24.3 (6.3)	21.0 (4.0)
No. of unique reflections	54,090 (5321)	17,781 (1744)	28,132 (2785)
Multiplicity	26.3 (25.6)	39.4 (40.3)	13.1 (13.3)
Completeness (%)	100.0 (100.0)	100.0 (100.0)	100.0 (100.0)
$CC_{1/2}$[b]	0.997 (0.947)	0.994 (0.969)	0.996 (0.974)
Wilson B-factor (Å^2)	26.4	41.6	33
Resolution (Å)	33.4–2.0 (2.08–2.0)	28.7–2.9 (3.0–2.9)	26.1–2.5 (2.59–2.5)
No. of unique reflections	54,009 (5172)	17,714 (1633)	27,972 (2736)
Completeness (%)	99.6 (97.0)	99.1 (92.1)	99.4 (98.2)
R_{work} (%)	15.9 (18.7)	18.4 (22.1)	17.8 (22.7)
R_{free} (%)	18.4 (22.8)	23.9 (29.1)	20.9 (28.02)
No. of atoms	6046	5529	5598
Protein	5449	5383	5259
Ligands	137	140	135
Solvent (H_2O)	460	6	204
RMS deviations			
Bond lengths (Å)	0.005	0.003	0.003
Bond angles (°)	0.86	0.69	0.72
B-factors (Å^2)			
Protein	33.3	40.3	39.9
Solvent and ligands	33.8	31.3	34.9
Ramachandran (%)			
Favored	97.2	95.2	97.1
Outliers	0.2	0.6	0.5
PDB[c] code	6NBE	6NAS	6NBW

a, Numbers in parenthesis correspond to highest resolution shell; b, Pearson's correlation coefficient; c, Protein Data Bank.

We then tested the effect of the mutations on the activity and interaction of NAA80 with full-length actin. By ITC, mutant M4, combining two groups of mutations (M1 and M2), did not bind Ac-α-actin (Fig. 4E). Consistently, mutant M4 was also unable to Nt-acetylate β/γ-actin purified from *NAA80* KO cells (Fig. 4F). The four mutants were then expressed in *NAA80* KO cells and their activities compared to that of WT NAA80 (Fig. 4G). Alone, mutants M1 and M2, but not M3, significantly reduced the ability of NAA80 to acetylate β- and γ-actin in cells. Mutant M4, targeting the actin-binding (M1) and profilin-binding (M3) surfaces, completely eliminated NAA80's ability to Nt-acetylate β- and γ-actin. These results show that NAA80 specifically recognizes its actin-profilin substrate through extensive surface contacts and not only the N terminus, as do other NATs. Moreover, while on its own, the profilin-binding site has weak affinity (Fig. 2F) and contributes little toward the catalytic activity (Fig. 4G), but together with other contacts on the actin surface, it adds to the exquisite specificity and enhanced activity of NAA80 for actin-profilin (Fig. 2G).

There is approximately one NAA80 molecule for every 3000 actin molecules in cells

Given the NAA80's exclusive specificity for actin, we asked what was the cellular ratio of enzyme to substrate. By calibrating the relative concentration of NAA80 and actin in protein lysates against purified proteins, we estimated that there is approximately one NAA80 enzyme per ~3000 actin molecules (Fig. 5). This relatively small amount of NAA80 appears nonetheless sufficient to Nt-acetylate the small population of newly translated actin, considering that actin has a long half-life in muscle sarcomeres (*23*) and nonmuscle cells (*24*) and ~100% of it is Nt-acetylated (*7*).

DISCUSSION

Actin occupies a special place in the cell; it is the most abundant protein in the cytoplasm, participates in more protein-protein interactions than any other protein, and is highly conserved (*13*, *14*). While the six actin isoforms diverge the most at the N terminus (Fig. 3B), they all have highly negative N termini (Fig. 4A), which distinguishes them from any other protein in the cell. Together, these characteristics may explain why animals use a dedicated enzyme to Nt-acetylate actin. Curiously, the only other substrate-dedicated NAT, NatD, Nt-acetylates histones H2A and H4 (*6*), which, along with actin, are among the most highly conserved proteins in nature. Nt-acetylation masks the positive charge of the α-amino group on actin, thus accentuating the overall negative charge of the N terminus, which is prominently exposed in the filament and participates in interactions with many ABPs (*9*). Consistently, the lack of actin Nt-acetylation has profound effects on filament assembly in cells, including increased filopodia and lamellipodia formation and faster cell migration, whereas, in vitro, it decreases the rates of filament depolymerization and formin-mediated elongation (*7*).

Despite ~80% of human proteins being Nt-acetylated, not a single NAT-substrate structure existed thus far, such that the NAA80-actin-profilin structures described here offer a rare look into the mechanism of Nt-acetylation. These structures reveal a rather unique case of enzyme-substrate adaptation, including (i) NAA80's preference for G- versus F-actin, which ensures that Nt-acetylation precedes polymerization, with the polymer being the functionally most relevant form of actin (Fig. 1 and fig. S2); (ii) NAA80's ability

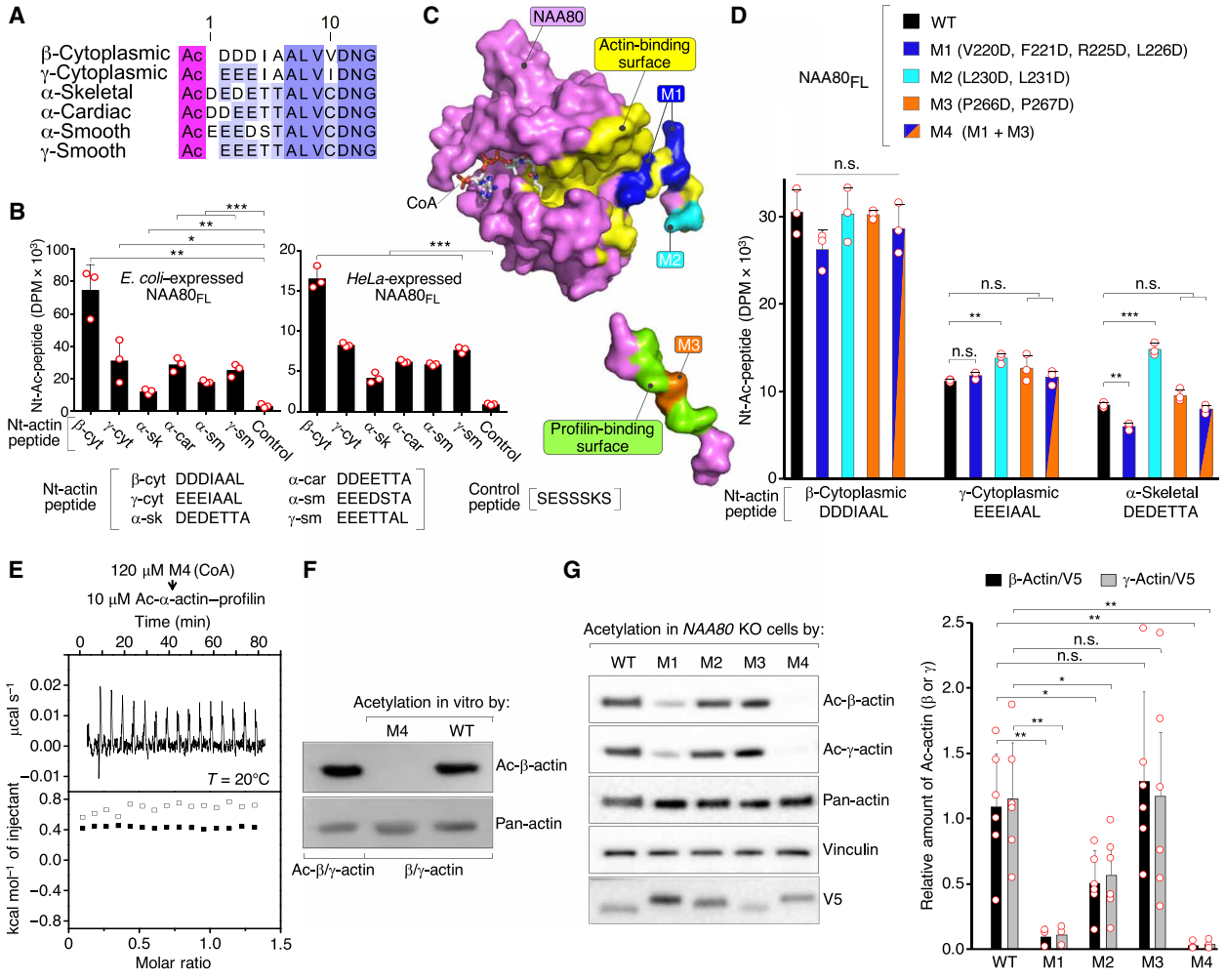

Fig. 4. NAA80 specifically recognizes actin-profilin through extensive surface contacts. (**A**) Alignment of the N-terminal sequences of the six human actin isoforms as they exist in cells after processing and Nt-acetylation. (**B**) *E. coli*– and mammalian cell–expressed NAA80 can acetylate N-terminal peptides derived from all six human actin isoforms but not a prototypical NatA/NAA10-substrate peptide, shown as a control (see fig. S9 for full peptide sequences and characterization). Acetylation is reported as the amount of radioactive product measured in disintegrations per minute (DPM). Error bars are ±SD ($n = 3$; red open circles). The statistical significance of the measurements was determined using an unpaired two-sided Student's t test, comparing each of the actin peptides to the control (*$P < 0.05$, **$P < 0.01$, ***$P < 0.001$). (**C**) Surface representation of the structure of NAA80, showing the actin-binding (yellow) and profilin-binding (green) interfaces and groups of residues replaced in mutants M1 (V220D, F221D, R225D, and L226D; blue), M2 (L230D and L231D; cyan), and M3 (P266D and P267D; orange). (**D**) In vitro activity of $NAA80_{FL}$ mutants M1, M2, M3, and M4 (M1 + M3) immunoprecipitated from HeLa cells toward N-terminal actin peptides (fig. S9). The activity was normalized against the expression level and immunoprecipitation efficiency of each construct. Error bars are ±SD ($n = 3$; red open circles). The statistical significance of the measurements was determined using an unpaired two-sided Student's t test (n.s., $P \geq 0.05$, **$P < 0.01$, ***$P < 0.001$). (**E**) ITC titrations of $NAA80_{FL}$ mutant M4 (CoA) into Ac-α-actin–profilin (LatB) using the indicated experimental conditions. The data could not be fit to a binding isotherm. Open symbols correspond to a control titration into buffer. (**F**) NAA80 mutant M4 cannot acetylate nonacetylated β/γ-actin, as monitored by Western blot analysis using acetylation- and isoform-specific anti–Ac-β-actin antibody. Shown as a control is Ac-β/γ-actin purified from WT cells, and loading is controlled by anti–pan-actin staining. (**G**) Rescue of β/γ-actin acetylation in *NAA80* KO cells transfected with V5-$NAA80_{FL}$ WT and mutants M1 to M4 analyzed by Western blot using acetylation- and isoform-specific anti-actin antibodies. Anti-V5 staining shows levels of NAA80 expression, whereas anti–pan-actin and anti-vinculin staining provide loading controls (see also fig. S2C). For each mutant, the intensities of the Ac-β-actin and Ac-γ-actin bands were first normalized to the expression level (V5 signal) and then to the level of WT Ac-β/γ-actin. Error bars are ±SD for $n = 6$ (WT, M2, and M3) or $n = 3$ (M1 and M4) independent experiments shown as red open circles. The statistical significance of the measurements was determined using a two-way analysis of variance (ANOVA) test between WT and each mutant (n.s., $P \geq 0.05$, *$P < 0.05$, **$P < 0.01$).

to recognize not only G-actin but also the actin-profilin complex, which is the most abundant form of G-actin in cells (Figs. 2 and 3); and (iii) an NAA80 structure specifically tailored to recognize the highly conserved actin surface and the relatively variable but negatively charged actin N terminus (Fig. 3 and fig. S4, A to C). Below, we expand on the implications of each of these observations.

The structures explain why the binding of NAA80 to Tpm-decorated actin filaments is unfavorable in cells (Fig. 1, D and E), despite taking place at lower affinity in vitro (Figs. 1F and 2C). Tpm can occupy three different positions on the actin filament (blocked, closed, and open), with the latter two being separated by azimuthal rotations of ~25° and ~10° with respect to the energetically more

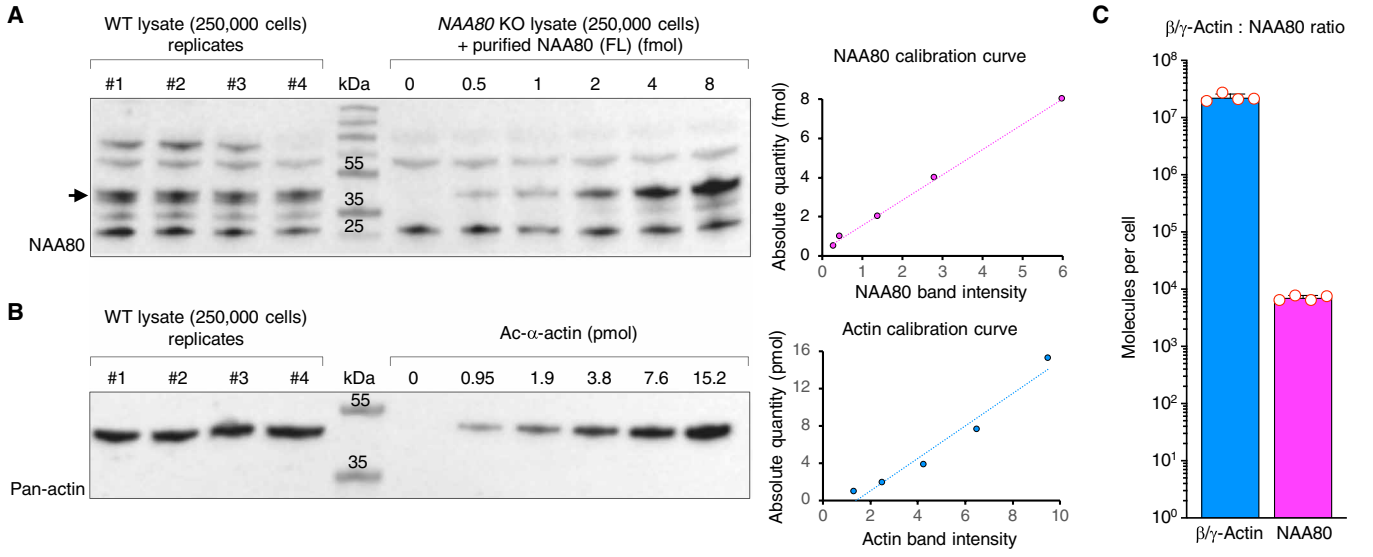

Fig. 5. There is one NAA80 molecule for every 3000 actin molecules in cells. (**A**) Western blot analysis of the amount of endogenous NAA80 in HAP1 WT cell lysates (left) compared to specific amounts of purified NAA80 added to *NAA80* KO HAP1 cell lysates (right) and the resulting standard curve. The arrow points to the NAA80 band detected by a custom-made antibody. (**B**) Western blot analysis of the amount of endogenous actin in HAP1 WT cell lysates (left) compared to specific amounts of purified actin (right) and the resulting standard curve. (**C**) Quantification of the absolute amounts of NAA80 and actin in HAP1 WT cells ($n = 4$). Errors correspond to the SD.

favorable blocked state (*25*). NAA80 overlaps with Tpm in the blocked state, so it can only bind to the filament after "pushing" Tpm to the closed or open states (fig. S6), which it can achieve but, at an energy cost, reflected in its lower affinity for Tpm-decorated filaments. It is less clear why NAA80 binds monomers with higher affinity than naked filaments. NAA80 does not appear to compete with either profilin or DNase I for binding to monomeric actin (Fig. 2, A and B, and fig. S3C), with the binding surfaces of these two proteins coinciding with the two major intersubunit contacts along the long-pitch helix of the filament (fig. S3D). One possibility is that NAA80's weaker affinity for the filament results from the conformational change that takes place upon actin polymerization (*26*). It is also possible that the Pro-rich insert of NAA80 partially hinders binding to filaments.

The structures also illuminate NAA80's preference for actin-profilin compared to actin alone. Thus, NAA80 is the only NAT that has a long proline-rich loop inserted before the last β-strand of the catalytic domain, featuring a canonical profilin-binding sequence (fig. S1A). We have shown here that NAA80 binds profilin directly (Fig. 2F) and that the interaction is mediated by the Pro-rich loop (Fig. 3A). We have further shown that profilin acts as a chaperone for actin Nt-acetylation (Fig. 2G) by significantly enhancing the Nt-acetylation efficiency of NAA80 toward the actin-profilin substrate.

NAA80 is distinguished from other NATs in that it has a wide open and positively charged substrate-binding cleft (fig. S5B), adapted to accommodate the variable, negatively charged N termini of actin isoforms (fig. S4, A to C). On the other hand, NAA80 presents a surface to the actin substrate entirely different from that of other NATs (Fig. 3C and fig. S5A). Together, the structural and functional features uncovered here explain why actin is NAA80's sole substrate in the cell and why, in its absence, no other NAT can Nt-acetylate actin, which constitutes a rather unique example of enzyme-substrate congruity.

MATERIALS AND METHODS

Proteins

The gene encoding human NAA80 (UniProt ID: Q93015-2) was obtained using Transcriptor Reverse Transcriptase (Roche) from human embryonic kidney 293 cells cDNA (complementary DNA) (*7*). For bacterial expression, $NAA80_{FL}$ and $NAA80_{\Delta N}$ (residues 78 to 308) were cloned between the *NdeI* and *XhoI* sites of vector pTYB12 [New England Biolabs (NEB)], which comprises a chitin-binding domain for affinity purification and an intein domain for self-cleavage of the affinity tag after purification. The M4 mutant (V220D, F221D, R225D, L226D, P266D, and P267D) was generated from $NAA80_{FL}$ using the QuickChange mutagenesis kit (Stratagene). The proteins were expressed in ArcticExpress(DE3) RIL cells (Agilent Technologies), grown in Terrific Broth (TB) medium for 6 hours at 37°C to a density of ~1.5 to 2 optical density at 600 nm (OD_{600}), followed by 24 hours at 10°C in the presence of 0.4 mM isopropyl-β-D-thiogalactoside (IPTG). Cells were harvested by centrifugation, resuspended in 20 mM Hepes (pH 7.5), 500 mM NaCl, 1 mM EDTA, and 1 mM phenylmethanesulfonyl fluoride (PMSF) and lysed using a microfluidizer (Microfluidics). The proteins were first purified on a chitin affinity column, according to the manufacturer's protocol (NEB), followed by ion exchange chromatography using a Mono S column (GE Healthcare) in 20 mM MES (pH 5.5 for NAA80 or pH 6.5 for $NAA80_{\Delta N}$) and a 50 to 1000 mM NaCl gradient. A final step of purification was performed on a gel filtration SD200HL 26/600 column (GE Healthcare) in 20 mM Hepes (pH 7.5) and 100 mM NaCl.

The cDNA encoding human profilin-1 (UniProt ID: P07737) was purchased from the American Type Culture Collection (ATCC) and cloned between the *SapI* and *EcoRI* sites of vector pTYB11 (NEB). Profilin was expressed in BL21(DE3) cells (Invitrogen), grown in TB medium at 37°C to a density of ~1.5 to 2 OD_{600}, followed by 16 hours at 20°C in the presence of 0.5 mM IPTG. Cells were harvested by centrifugation, resuspended in 20 mM Hepes

(pH 7.5), 500 mM NaCl, 1 mM EDTA, and 1 mM PMSF, and lysed using a microfluidizer. The protein was purified on a chitin affinity column, according to the manufacturer's protocol, followed by gel filtration on a SD75HL 16/600 column (GE Healthcare) in 20 mM Hepes (pH 7.5) and 100 mM NaCl.

The cDNA encoding human gelsolin (UniProt ID: P06396) was purchased from Open Biosystems (GE Healthcare). Gelsolin subdomain 1 (also called GS1, residues 1 to 125) was cloned between the *NdeI* and *EcoRI* sites of vector pTYB12 and expressed and purified as described for profilin above. The fragment encoding gelsolin subdomains 4 to 6 GS4-GS6, residues 434 to 782) was cloned between the *XhoI* and *EcoRI* sites of vector pCold I (Clontech Laboratories) and expressed in Rosetta (DE3) cells (Novagen). Cells were grown in TB medium at 37°C to a density of 0.8 OD_{600}, followed by 24 hours at 15°C in the presence of 0.3 mM IPTG. Cells were harvested by centrifugation, resuspended in 50 mM tris-HCl (pH 8.0), 500 mM NaCl, 5 mM imidazole, and 1 mM PMSF, lysed using a microfluidizer, and purified on a Ni–NTA (nitrilotriacetic acid) affinity column (QIAGEN) according to the manufacturer's protocol.

Ac-β/γ-actin and non-Ac-β/γ-actin were purified from WT and *NAA80* KO HAP1 cells (Horizon Discovery), respectively, using GS4-GS6's calcium-activated switch (*27*) as an affinity purification method, as we previously described (*7*). Ac-α-actin and Tpm were purified from rabbit skeletal muscle as previously described (*28*).

The plasmid (EGPF-N backbone) carrying human β-actin–Tβ4 hybrid with C-terminal His-tag was a gift from H. Higgs (Dartmouth Medical School). The hybrid construct was expressed in a 100-ml culture of mammalian Expi293 cells and purified on a Ni-NTA affinity column according to the manufacturer's protocol. DNase I was purchased from VWR.

The concentration of NAA80 and its complexes with actin and actin-profilin were determined using the Coomassie Plus (Bradford) assay (Thermo Fisher Scientific). The concentration of actin was determined spectrophotometrically at 290 using extinction coefficient of 26,600 M^{-1} cm^{-1}. The concentration of other proteins was determined at 280 nm, using the following coefficients: profilin1, 18,450 M^{-1} cm^{-1}; GS1, 21,430 M^{-1} cm^{-1}; GS4-GS6, 65,890 M^{-1} cm^{-1}; DNase1, 38,850 M^{-1} cm^{-1}; Tpm, 8940 M^{-1} cm^{-1}.

Plasmids for mammalian cell expression

The *NAA80* gene was inserted into vector pcDNA3.1/V5-His TOPO TA (Invitrogen), as we have described (*7*). The catalytically inactive mutant $NAA80_{CM}$ (W105F, R170Q, G173D, and Y205F) and other mutants (Fig. 4D) were generated using the Q5 Site-Directed Mutagenesis Kit (NEB). The NAA80 constructs were cloned into vector pcDNA4/HisMax TOPO TA (Invitrogen), in which the Xpress tag was replaced with a V5 tag. For imaging, $NAA80_{FL}$ and $NAA80_{\Delta N}$ were cloned between the *BglII* and *HindIII* sites of vector EGFP-C1 (Clontech Laboratories).

Human cell culture

HAP1 WT and *NAA80* KO cells (Horizon Discovery) were grown in Iscove's modified Dulbecco's medium, 10% fetal bovine serum (FBS), and 1% penicillin-streptomycin at 37°C and 5% CO_2. Cells were passaged and their diploid status confirmed on an Accuri BD C6 flow cytometer using propidium iodide staining. HeLa cells (ATCC) were cultured in Dulbecco's modified Eagle's medium, 10% FBS, and 1% penicillin-streptomycin. Cells were seeded on plates or coverslips and transfected with X-tremeGENE 9 (Roche) or FuGENE (Promega). Cells were harvested, imaged alive, or fixed 24 to 48 hours after transfection.

Immunofluorescence

HeLa, HAP1 WT, or *NAA80* KO cells were transfected with 1 μg of GFP-NAA80, with or without cotransfection with mCherry empty vector, and fixed 48 hours after transfection with 4% (w/v) paraformaldehyde for 10 min. For F-actin visualization, cells were permeabilized with 0.5% Tween 20 [in phosphate-buffered saline (PBS)] for 15 min and incubated with 100 nM Alexa Fluor 546 phalloidin (Invitrogen) for 30 min at room temperature (RT). Coverslips were mounted on a drop of ProLong Diamond Antifade Mountant (Invitrogen) and imaged within 48 hours, using an Eclipse TE2000-U inverted microscope (Nikon) equipped with a PlanApo 100×/1.3 numerical aperture objective and a Cascade 512B charge-coupled device camera (Photometrics) controlled by the MetaMorph imaging software (Molecular Devices). The images were level-adjusted with Adobe Photoshop. Line-scans were taken with the program Fiji (ImageJ).

For live-cell imaging, HeLa cells were transfected with 1 μg of GFP-NAA80, together with one of the following markers: mCherry-LifeAct, DsRed-Mito, mCherry-Sec61B, or mCherry-Calnexin. The cells were imaged 24 hours after transfection using the same microscope.

Cell fractionation assay

HAP1 WT and *NAA80* KO cells were harvested by scraping and resuspended in 750 μl of prewarmed LAS buffer [50 mM Pipes (pH 6.9), 50 mM NaCl, 5 mM $MgCl_2$, 5 mM EGTA, 5% (v/v) glycerol, 0.1% NP-40, 0.1% Triton X-100, 0.1% Tween 20, 0.1% β-mercaptoethanol, 1 mM ATP, 0.001% Antifoam C, and a protease inhibitor cocktail consisting of 0.4 mM tosyl arginine methyl ester, 1.5 mM leupeptin, 1 mM pepstatin A, and 1 mM benzamidine]. Cells were lysed using the EMBL (European Molecular Biology Laboratory) cell cracker (ball size, 8.010 mm) with 16 strokes or by 10 passages through a 25-gauge needle. The lysate was clarified by centrifugation (400*g* for 5 min at RT). The supernatant (100 μl) was collected, and actin polymerization was initiated by addition of 2 mM $MgCl_2$, 0.2 mM EGTA, 100 mM KCl, and 1 μM phalloidin and by incubation for 1 hour at 37°C. F-actin and F-actin–binding proteins were pelleted by ultracentrifugation (270,000*g* for 1 hour at 4°C). The supernatant (G-actin fraction) was collected, and the pellet (F-actin fraction) was washed twice with Milli-Q water and resuspended in 100 μl of 8 M urea. After addition of SDS loading buffer, the samples were separated by SDS–polyacrylamide gel electrophoresis (PAGE) and analyzed by Western blotting, using the following antibodies: custom anti-NAA80 polyclonal rabbit (1:200; BioGenes, Germany), anti–pan-actin polyclonal rabbit (1:2000; Cell Signaling Technology, 4968), anti-mDia1 monoclonal rabbit (1:2000; Abcam, ab129167), anti-profilin monoclonal rabbit (1:2000; Abcam, ab50667).

For the experiment with V5-tagged NAA80 constructs, cells were transfected with 2 to 6 μg of V5-$NAA80_{FL}$, $NAA80_{CM}$-V5 (catalytically inactive mutant), or V5-$NAA80_{\Delta N}$. The same number of cells per cell line (2×10^6) was washed briefly 24 hours after transfection with PBS and processed as above. In the Western blotting analysis, anti-V5 monoclonal mouse antibody (1:1000; Invitrogen, R960CUS) was used instead of anti-NAA80 antibody.

In vitro acetylation of actin and actin-profilin

Non–Ac-β/γ-actin (purified from *NAA80* KO cells) at 10 μM in G-buffer, alone or in complex with profilin (prepared by mixing at 1:1.2 molar ratio), was incubated with *E. coli*–expressed $NAA80_{FL}$ at molar ratios of 1:50, 1:100, 1:200, and 1:400 (NAA80:actin) and 50 μM AcCoA. At the indicated time points (5, 10, 20, and 60 min; Fig. 2G and fig. S8), 10 μl of each sample was transferred to 10 μl of SDS-PAGE loading buffer. The samples were analyzed by Western blotting using isoform- and acetylation-specific mouse monoclonal anti–Ac-β-actin (1:5000; Abcam, ab6276) and rabbit polyclonal anti–pan-actin (1:2000; Cell Signaling Technology, 4968) antibodies. Densitometric analysis was performed using a G:BOX scanner (Syngene) and the Image Lab 6.0.1 software (Bio-Rad). For each blot, the band intensities were normalized to the 1:50 NAA80:actin-profilin band, which was always the strongest. Mean relative intensities and SD were calculated from three independent experiments ($n = 3$).

Immunoprecipitation of NAA80 constructs

For immunoprecipitation of V5-NAA80 constructs, 7.5×10^6 HeLa cells were transfected with 12 μg of DNA and X-tremeGENE 9. After 24 hours, cells were harvested and lysed in 1.2 ml of IPH buffer [50 mM tris-HCl (pH 8.0), 150 mM NaCl, 0.1% NP-40, and EDTA-free protease inhibitor cocktail (Roche)] for 15 min at 4°C. Lysates were clarified by centrifugation (17,000*g* for 15 min at 4°C). The supernatants were incubated for 4 hours at 4°C with 6 μg of anti-V5 antibody (Invitrogen, R960CUS), followed by the addition of 25 μl of Protein A/G Mix Magnetic Beads (Millipore), and washed three times in IPH buffer. After incubation for 16 hours and washing two times in IPH buffer and once in acetylation buffer [50 mM tris-HCl pH 7.4, 1 mM EDTA, 1 mM dithiothreitol (DTT), and 10% (v/v) glycerol], the samples were used in [^{14}C]-Ac-CoA peptide acetylation assays.

[^{14}C]-AcCoA–based peptide acetylation assay

The peptide acetylation assay was performed as we have described (*7*, *29*). Briefly, NAA80 (*E. coli*–expressed or immunoprecipitated from HeLa cells) was mixed with 300 μM synthetic peptides (synthesized and quality-controlled by BioGenes; fig. S9) and 50 μM isotope-labeled [^{14}C]-AcCoA (PerkinElmer) in a total volume of 25 μl of acetylation buffer (see above). The samples were incubated for 1 hour at 37°C, and 20 μl was then transferred onto P81 phosphocellulose filter discs (Millipore). The discs were washed three times with 10 mM Hepes (pH 7.4) and dried before they were added to 5 ml of scintillation cocktail Ultima Gold F (PerkinElmer). The amount of incorporated [^{14}C]-Ac was determined by a Tri-Carb 2900TR Liquid Scintillation Analyzer (PerkinElmer). The activity was corrected for the amount of immunoprecipitated NAA80 determined by Western blot analysis.

Rescue of actin acetylation in *NAA80* KO cells

NAA80 KO cells were split 1:3, seeded in 10-cm plates, cultured overnight, and transfected with varying amounts of V5-NAA80 WT and mutant (M1 to M4) DNA as follows: WT, 12 μg, $n = 6$; M1 (V220D, F221D, R225D, and L226D), 2.1 μg, $n = 3$; M2 (L230D and L231D), 12 μg, $n = 6$; M3 (P266D and P267D), 1.5 μg, $n = 6$; M4 (V220D, F221D, R225D, L226D, P266D, and P267D), 4 μg, $n = 3$. Cells were harvested by trypsinization after 16 hours and lysed in IPH buffer (see above), and lysates were clarified by centrifugation at 17,000*g* for 5 min. The clarified lysates were loaded onto 8 to 16% SDS-PAGE gels (Bio-Rad) and run for 35 min at 200 V. Gels were transferred to polyvinylidene difluoride membrane and probed with anti–Ac-β-actin (monoclonal mouse, 1:5000; Abcam, ab6276), anti–Ac-γ-actin (monoclonal mouse, 1:5000; Abcam, ab123034), anti–pan-actin (polyclonal rabbit, 1:2000; Cell Signaling Technology, 4968), anti-V5 (monoclonal mouse, 1:3000; Invitrogen, R960CUS), and anti-vinculin (monoclonal rabbit, 1:1000 to 2000; Abcam, ab129002) antibodies. The densitometric analysis of the signal from horseradish peroxidase–conjugated secondary antibodies was performed using Image Lab 6.0.1 software (Bio-Rad). For each NAA80 variant, the bands for Ac-β-actin, Ac-γ-actin, and V5 were quantified relative to the WT signal. To account for the different expression levels of NAA80 mutants, Ac-β-actin and Ac-γ-actin signals were divided by the corresponding V5 signal. The SD for the ratio was calculated according to the following formula: $SD_{ratio} = \left(\frac{actin}{V5}\right) \times \sqrt{(CV_{actin})^2 + (CV_{V5})^2}$, where $CV = \frac{SD}{mean}$ of the V5 or actin signals. The means were compared using a two-way analysis of variance (ANOVA) with Dunnett's multiple comparison test and a significance threshold of 0.05 for the adjusted *P* value (GraphPad Software).

Quantification of NAA80 and actin abundance in cells

The quantification of NAA80 and actin was performed in WT HAP1 cells. For NAA80, a standard curve was first obtained by adding known amounts of *E. coli*–expressed $NAA80_{FL}$ to lysates from a specific number of HAP1 *NAA80* KO cells. For actin, a standard curve was obtained using known amounts of tissue-purified Ac-α-actin. For the quantification of NAA80, a custom antibody was raised against *E. coli*–expressed, tag-free $NAA80_{\Delta N}$ (polyclonal rabbit, 1:500; BioGenes, Germany), whereas actin was quantified using a commercial anti–pan-actin antibody (monoclonal mouse, 1:2000; Abcam, ab14128). Cell pellets were resuspended and lysed by incubation in IPH buffer (see above) for 20 min on ice, followed by centrifugation for 5 min at 17,000*g*. The standard curves and samples ($n = 4$) were quantified by Western blotting and densitometry analyses.

Isothermal titration calorimetry

ITC measurements were carried out on a VP-ITC apparatus (MicroCal). Before the experiments, samples were dialyzed for 2 days against 20 mM Hepes (pH 7.5), 100 mM NaCl, 0.2 mM ATP, and 1 mM DTT (ITC buffer). In experiments with NAA80, CoA or AcCoA (as indicated in the figures) was added to the buffer at 1.5 molar excess over the NAA80 concentration. In experiments with actin and actin-profilin, LatB was added to the buffer at a 1.2 molar excess over the actin concentration. The actin-profilin complex was prepared by mixing actin and profilin-1 at a 1:1.2 molar ratio. The higher-affinity complexes of actin-GS1 and actin–DNase I were prepared by mixing at a molar ratio of 1:1.5, followed by purification by gel filtration on a SD200HL 26/600 column (GE Healthcare) in ITC buffer to remove the excess of GS1 or DNase I. The experiments were carried out at 20°C, except for the titration of profilin into ΔN, whose weaker binding yielded a stronger signal at 30°C. Titrations consisted of 10-μl injections, lasting for 10 s, with an interval of 300 s between injections. The concentrations of the proteins in the syringe and the cell (volume of 1.44 ml) are listed in the figures. The heat of binding was corrected for the heat of injection, determined by injecting titrant into buffer (open symbols in figures). Data were analyzed using the program Origin (OriginLab Corporation).

F-actin cosedimentation assay

Actin at 20 μM in G-buffer was polymerized by the addition of 100 mM KCl, 2 mM $MgCl_2$, and 1 mM EGTA and incubation for 30 min at RT. Tpm-decorated actin filaments were formed by the addition of 6.3 μM Tpm (actin:Tpm ratio of 3.2:1). Cofilin-decorated filaments were formed by addition of 5× molar excess of human cofilin 2. Before the experiments, NAA80 in 20 mM Hepes (pH 7.5) and 100 mM NaCl (NAA80 buffer) was centrifuged at 278,000*g* for 30 min to remove aggregates. The samples were prepared by mixing a fixed concentration of F-actin (4 μM ± 1.2 μM Tpm) with increasing concentrations of NAA80 (0 to 24 μM) and adjusting the sample volume to 150 μl with NAA80 buffer (n = 3 for each concentration). The samples were incubated for 1 hour at RT and pelleted by centrifugation at 278,000*g* for 30 min. The supernatant was collected, and the pellet was gently washed with 150 μl of NAA80 buffer and then resuspended in 150 μl (same buffer). Equal volumes of supernatant and resuspended pellet fractions were analyzed by SDS-PAGE (fig. S7). The densitometric analysis of the bands in the gels was performed using a G:Box gel scanner (Syngene) and the program GelBandFitter, designed to analyze closely spaced bands (*30*). The ratio of NAA80 bound to F-actin was determined from the ratio of the corresponding band intensities in the same pellet lane, corrected for the percentage of actin in the supernatant lane. The data were fitted with the equation $\frac{[\mathrm{NAA\,80_{bound}}]}{[\text{F-actin}]} = B_{\max}\frac{[\mathrm{NAA\,80_{free}}]}{(K_D + [\mathrm{NAA\,80_{free}}])}$, in which $[\mathrm{NAA80_{free}}]$ is $[\mathrm{NAA80_{total}}] - [\mathrm{NAA80_{bound}}]$ and the $\frac{[\mathrm{NAA\,80_{bound}}]}{[\text{F-actin}]}$ ratio was expressed as a function of $[\mathrm{NAA80_{total}}]$. The calculations were performed using the program Origin. SEM values were determined from three independent experiments (fig. S7).

Crystallography

The complexes of β/γ-actin/profilin/$\mathrm{NAA80_{\Delta N}}$-AnCoA, Ac-α-actin–profilin–$\mathrm{NAA80_{\Delta N}}$-CoA, and Ac-α-actin–profilin/$\mathrm{NAA80_{\Delta N}}$-AcCoA were formed by mixing the three proteins at 1:1.2:1.2 molar ratio in 20 mM Hepes (pH 7.5), 50 mM NaCl, 0.2 mM ATP, 0.2 mM $CaCl_2$, 1 mM DTT, and 50 μM LatB. The concentration of the NAA80 cofactors (AnCoA, CoA, and AcCoA) was 150 μM. AnCoA was a gift from R. Marmorstein (University of Pennsylvania). The complexes were concentrated to 3 to 4 mg ml^{-1} using Amicon Ultra centrifugal filters (Millipore). Before crystallization, samples were centrifuged at 278,000*g* for 30 min to remove potential aggregates. Crystals were obtained at 16°C using the hanging drop vapor diffusion method. The crystallization drops at 2 μl consisted of a 1:1 (v/v) mixture of protein solution and a well solution containing 100 mM MES (pH 6.5), 200 mM NH_4NO_3, and 16% (v/v) polyethylene glycol 3350. Crystal quality was improved through successive rounds of microseeding using an Oryx4 crystallization robot (Douglas Instruments). For data collection, crystals were flash-frozen in liquid nitrogen from a cryo-solution consisting of well buffer and 30% (v/v) glycerol.

X-ray diffraction datasets were collected at 100 K at beamline F1 (MacCHESS, Cornell University). The datasets were indexed and scaled with the program HKL2000 (HKL Research). The structures were determined by molecular replacement, using as a search model, the 1.5-Å resolution structure of actin-profilin with a VASP fragment [Protein Data Bank (PDB) entry 2PBD (*18*)]. Model building and refinement were performed with the programs Coot (*31*) and Phenix (*32*), respectively. Figures of the structures were prepared with the program PyMOL (Schrödinger).

Statistical methods

The statistical significance of the measurements was determined using an unpaired two-way Student's t test or a two-way ANOVA test, both implemented in the program Prism v8.1.2 (GraphPad Software). The results were deemed nonsignificant (n.s.) for $P \geq 0.05$. The details are reported in the figure legends.

SUPPLEMENTARY MATERIALS

Supplementary material for this article is available at http://advances.sciencemag.org/cgi/content/full/6/15/eaay8793/DC1

View/request a protocol for this paper from *Bio-protocol*.

REFERENCES AND NOTES

1. T. Arnesen, P. Van Damme, B. Polevoda, K. Helsens, R. Evjenth, N. Colaert, J. E. Varhaug, J. Vandekerckhove, J. R. Lillehaug, F. Sherman, K. Gevaert, Proteomics analyses reveal the evolutionary conservation and divergence of N-terminal acetyltransferases from yeast and humans. *Proc. Natl. Acad. Sci. U.S.A.* **106**, 8157–8162 (2009).
2. H. Aksnes, A. Drazic, M. Marie, T. Arnesen, First things first: Vital protein marks by N-terminal acetyltransferases. *Trends Biochem. Sci.* **41**, 746–760 (2016).
3. S.-E. Park, J.-M. Kim, O.-H. Seok, H. Cho, B. Wadas, S.-Y. Kim, A. Varshavsky, C.-S. Hwang, Control of mammalian G protein signaling by N-terminal acetylation and the N-end rule pathway. *Science* **347**, 1249–1252 (2015).
4. H. Aksnes, R. Ree, T. Arnesen, Co-translational, post-translational, and non-catalytic roles of N-terminal acetyltransferases. *Mol. Cell* **73**, 1097–1114 (2019).
5. H. Aksnes, P. Van Damme, M. Goris, K. K. Starheim, M. Marie, S. I. Stove, C. Hoel, T. V. Kalvik, K. Hole, N. Glomnes, C. Furnes, S. Ljostveit, M. Ziegler, M. Niere, K. Gevaert, T. Arnesen, An organellar nalpha-acetyltransferase, naa60, acetylates cytosolic N termini of transmembrane proteins and maintains Golgi integrity. *Cell Rep.* **10**, 1362–1374 (2015).
6. K. Hole, P. Van Damme, M. Dalva, H. Aksnes, N. Glomnes, J. E. Varhaug, J. R. Lillehaug, K. Gevaert, T. Arnesen, The human N-alpha-acetyltransferase 40 (hNaa40p/hNatD) is conserved from yeast and N-terminally acetylates histones H2A and H4. *PLOS ONE* **6**, e24713 (2011).
7. A. Drazic, H. Aksnes, M. Marie, M. Boczkowska, S. Varland, E. Timmerman, H. Foyn, N. Glomnes, G. Rebowski, F. Impens, K. Gevaert, R. Dominguez, T. Arnesen, NAA80 is actin's N-terminal acetyltransferase and regulates cytoskeleton assembly and cell motility. *Proc. Natl. Acad. Sci. U.S.A.* **115**, 4399–4404 (2018).
8. P. A. Rubenstein, K.-k. Wen, NATure of actin amino-terminal acetylation. *Proc. Natl. Acad. Sci. U.S.A.* **115**, 4314–4316 (2018).
9. T. Arnesen, R. Marmorstein, R. Dominguez, Actin's N-terminal acetyltransferase uncovered. *Cytoskeleton* **75**, 318–322 (2018).
10. S. Varland, J. Vandekerckhove, A. Drazic, Actin post-translational modifications: The Cinderella of cytoskeletal control. *Trends Biochem. Sci.* **44**, 502–516 (2019).
11. J. C. M. Meiring, N. S. Bryce, Y. Wang, M. H. Taft, D. J. Manstein, S. Liu Lau, J. Stear, E. C. Hardeman, P. W. Gunning, Co-polymers of actin and tropomyosin account for a major fraction of the human actin cytoskeleton. *Curr. Biol.* **28**, 2331–2337.e5 (2018).
12. R. Dominguez, Tropomyosin: The gatekeeper's view of the actin filament revealed. *Biophys. J.* **100**, 797–798 (2011).
13. T. D. Pollard, What we know and do not know about actin. *Handb. Exp. Pharmacol.* **235**, 331–347 (2017).
14. R. Dominguez, K. C. Holmes, Actin structure and function. *Annu. Rev. Biophys.* **40**, 169–186 (2011).
15. V. K. Vinson, E. M. De La Cruz, H. N. Higgs, T. D. Pollard, Interactions of Acanthamoeba profilin with actin and nucleotides bound to actin. *Biochemistry* **37**, 10871–10880 (1998).
16. B. Xue, C. Leyrat, J. M. Grimes, R. C. Robinson, Structural basis of thymosin-beta4/profilin exchange leading to actin filament polymerization. *Proc. Natl. Acad. Sci. U.S.A.* **111**, E4596–E4605 (2014).
17. R. Dominguez, The WH2 domain and actin nucleation: Necessary but insufficient. *Trends Biochem. Sci.* **41**, 478–490 (2016).
18. F. Ferron, G. Rebowski, S. H. Lee, R. Dominguez, Structural basis for the recruitment of profilin-actin complexes during filament elongation by Ena/VASP. *EMBO J.* **26**, 4597–4606 (2007).
19. E. C. Petrella, L. M. Machesky, D. A. Kaiser, T. D. Pollard, Structural requirements and thermodynamics of the interaction of proline peptides with profilin. *Biochemistry* **35**, 16535–16543 (1996).
20. S. Y. Khaitlina, Functional specificity of actin isoforms. *Int. Rev. Cytol.* **202**, 35–98 (2001).
21. M. Goris, R. S. Magin, H. Foyn, L. M. Myklebust, S. Varland, R. Ree, A. Drazic, P. Bhambra, S. I. Støve, M. Baumann, B. E. Haug, R. Marmorstein, T. Arnesen, Structural determinants

and cellular environment define processed actin as the sole substrate of the N-terminal acetyltransferase NAA80. *Proc. Natl. Acad. Sci. U.S.A.* **115**, 4405–4410 (2018).
22. E. Wiame, G. Tahay, D. Tyteca, D. Vertommen, V. Stroobant, G. T. Bommer, E. Van Schaftingen, NAT6 acetylates the N-terminus of different forms of actin. *FEBS J.* **285**, 3299–3316 (2018).
23. B. Russell, D. Motlagh, W. W. Ashley, Form follows function: How muscle shape is regulated by work. *J. Appl. Physiol.* **88**, 1127–1132 (2000).
24. N. Rubinstein, J. Chi, H. Holtzer, Coordinated synthesis and degradation of actin and myosin in a variety of myogenic and non-myogenic cells. *Exp. Cell Res.* **97**, 387–393 (1976).
25. W. Lehman, Thin filament structure and the steric blocking model. *Compr. Physiol.* **6**, 1043–1069 (2016).
26. S. Z. Chou, T. D. Pollard, Mechanism of actin polymerization revealed by cryo-EM structures of actin filaments with three different bound nucleotides. *Proc. Natl. Acad. Sci. U.S.A.* **116**, 4265–4274 (2019).
27. R. C. Robinson, M. Mejillano, V. P. Le, L. D. Burtnick, H. L. Yin, S. Choe, Domain movement in gelsolin: A calcium-activated switch. *Science* **286**, 1939–1942 (1999).
28. J. D. Pardee, J. A. Spudich, Purification of muscle actin. *Methods Enzymol.* **85** (Pt B), 164–181 (1982).
29. A. Drazic, T. Arnesen, [^{14}C]-acetyl-coenzyme a-based in vitro N-terminal acetylation assay. *Methods Mol. Biol.* **1574**, 1–8 (2017).
30. M. I. Mitov, M. L. Greaser, K. S. Campbell, GelBandFitter—A computer program for analysis of closely spaced electrophoretic and immunoblotted bands. *Electrophoresis* **30**, 848–851 (2009).
31. P. Emsley, B. Lohkamp, W. G. Scott, K. Cowtan, Features and development of Coot. *Acta Crystallogr. D* **66**, 486–501 (2010).
32. P. D. Adams, P. V. Afonine, G. Bunkoczi, V. B. Chen, N. Echols, J. J. Headd, L. W. Hung, S. Jain, G. J. Kapral, R. W. Grosse Kunstleve, A. J. McCoy, N. W. Moriarty, R. D. Oeffner, R. J. Read, D. C. Richardson, J. S. Richardson, T. C. Terwilliger, P. H. Zwart, The Phenix software for automated determination of macromolecular structures. *Methods* **55**, 94–106 (2011).
33. J. Pei, N. V. Grishin, PROMALS3D: Multiple protein sequence alignment enhanced with evolutionary and three-dimensional structural information. *Methods Mol. Biol.* **1079**, 263–271 (2014).
34. L. A. Kelley, S. Mezulis, C. M. Yates, M. N. Wass, M. J. Sternberg, The Phyre2 web portal for protein modeling, prediction and analysis. *Nat. Protoc.* **10**, 845–858 (2015).
35. A. M. Waterhouse, J. B. Procter, D. M. Martin, M. Clamp, G. J. Barton, Jalview Version 2—A multiple sequence alignment editor and analysis workbench. *Bioinformatics* **25**, 1189–1191 (2009).
36. W. S. J. Valdar, Scoring residue conservation. *Proteins* **48**, 227–241 (2002).

Acknowledgments
Funding: This work was supported by NIH grants R01 GM073791 and R01 MH087950 to R.D. and by Research Council of Norway grants 230865 and 249843, Norwegian Cancer Society, Helse Vest, and European Research Council Horizon 2020 grant 772039 to T.A. **Author contributions:** R.D. conceived and directed the project, performed experiments, analyzed data, prepared figures, and wrote the paper with input from all the authors. G.R., M.B., A.D., R.R., M.G., and T.A. designed and performed experiments, analyzed data, and prepared data for publication. **Competing interests:** The authors declare that they have no competing interests. **Data and materials availability:** All data needed to evaluate the conclusions in the paper are present in the paper and/or the Supplementary Materials. Additional data related to this paper maybe requested from the authors. The crystal structures were deposited in the PDB (accession codes: 6NBW, 6NBE, and 6NAS).

Submitted 25 July 2019
Accepted 14 January 2020
Published 8 April 2020
10.1126/sciadv.aay8793

Citation: G. Rebowski, M. Boczkowska, A. Drazic, R. Ree, M. Goris, T. Arnesen, R. Dominguez, Mechanism of actin N-terminal acetylation. *Sci. Adv.* **6**, eaay8793 (2020).

Science Advances

Mechanism of actin N-terminal acetylation

Grzegorz Rebowski, Malgorzata Boczkowska, Adrian Drazic, Rasmus Ree, Marianne Goris, Thomas Arnesen and Roberto Dominguez

Sci Adv **6** (15), eaay8793.
DOI: 10.1126/sciadv.aay8793